

Article

Analysis and 3D Imaging of Multidimensional Complex THz Fields and 3D Diagnostics Using 3D Visualization via Light Field

Michael Gerasimov ^{1,2,*}, Adnan Haj Yahya ^{2,3}, Vadim Patrick Nave ³, Egor Dyunin ², Jacob Gerasimov ^{1,2,3} and Aharon Friedman ^{1,2}

¹ Department of Electrical and Electronic Engineering, Ariel University, Ariel 40700, Israel; jacobgr@ariel.ac.il (J.G.); aharonfr@ariel.ac.il (A.F.)

² The Schlesinger Family Center for Compact Accelerators, Radiation Sources & Applications (FEL), Ariel 40700, Israel; adnanhy@ariel.ac.il (A.H.Y.); edyunin@gmail.com (E.D.)

³ Department of Physics, Ariel University, Ariel 40700, Israel; nave9595@gmail.com

* Correspondence: michaelge@ariel.ac.il

[†] These authors contributed equally to this work.

Abstract: We present a numerical platform for 3D imaging and general analysis of multidimensional complex THz fields. A special 3D visualization is obtained by converting electromagnetic (EM) radiation to a light field via the Wigner distribution function, which is known for discovering (revealing) hidden details. This allows for 3D diagnostics using the simple techniques of geometrical optics, which significantly facilitates the whole analysis. This simulation was applied to a complex field composed of complex beams emitted as ultra-narrow femtosecond pulses. A method was developed for the generation of phase–amplitude and spectral characteristics of complex multimode radiation in a free-electron laser (FEL) operating under various parameters. The tool was successful at diagnosing an early design of the transmission line (TL) of an innovative accelerator at the Schlesinger Family Center for Compact Accelerators, Radiation Sources, and Applications.

Keywords: wigner distribution function (WDF); light field; FEL; 3D visualization; diagnostics; THz; terahertz radiation; compact accelerators; transmission line; homemade code



Citation: Gerasimov, M.; Yahya, A.H.; Nave, V.P.; Dyunin, E.; Gerasimov, J.; Friedman, A. Analysis and 3D Imaging of Multidimensional Complex THz Fields and 3D Diagnostics Using 3D Visualization via Light Field. *Computation* **2023**, *11*, 160. <https://doi.org/10.3390/computation11080160>

Academic Editors: José Antonio Marmolejo Saucedo, Joshua Thomas, Leo Mrsic, Román Rodríguez Aguilar and Pandian Vasant

Received: 30 May 2023

Revised: 3 August 2023

Accepted: 10 August 2023

Published: 14 August 2023



Copyright: © 2023 by the authors. Licensee MDPI, Basel, Switzerland. This article is an open access article distributed under the terms and conditions of the Creative Commons Attribution (CC BY) license (<https://creativecommons.org/licenses/by/4.0/>).

1. Introduction

Studies in the field of terahertz (THz) radiation have been gaining momentum recently, leading to greater demand for the development of THz radiation sources. In addition, THz research and applications have become widely popular and accessible [1,2]. Recent research has shown that THz radiation is not ionizing; therefore, it is environmentally friendly and not dangerous to biological organisms [3,4]. THz radiation can be transmitted through various types of media, such as wood, ceramic, plastic, textiles, paper, all-silicon metasurface [5,6] and transmissive THz metamaterial [7,8]. THz radiation enables nondestructive analysis of internal and even hidden substances. Therefore, it is expected to lead to the development of novel methods of nondestructive detection. THz radiation is generally defined as being within the region of the electromagnetic (EM) spectrum in the range of 100 GHz (3 mm) to 10 THz (30 μm), which is between millimeter and infrared frequencies. Hence, it has properties of light waves on the one hand and millimeter waves on the other. Today, there is almost no scientific or commercial field that is not interested in applying THz radiation [1]; some important fields include space, military, security, medicine, aviation, land exploration, 6G communications, and super-fast internet. At the same time, there is almost no precise equipment for working with THz because it is a new scientific field and still being researched, with an emphasis on detecting THz in general and displaying it on instrumentation in particular, such as radio waves on an oscilloscope, signals on a

spectrum analyzer, or laser radiation in optics. The Schlesinger Family Center for Compact Accelerators, Radiation Sources, and Applications faces exactly such a challenge in the field of compact accelerators: the development and construction of an advanced accelerator.

The aim of this study was to develop unique homemade simulations in order to assess the radiation dynamics of the propagation of wideband ultra-short THz pulses in free space and in a specific transmission line (TL) using light field [9] (LF) representation methods and to study the TL's predesign by complex diagnostics for the advanced free-electron laser (FEL) under construction.

To achieve this goal, the following tasks were formulated:

1. Analyze the energy spectral density distribution (dW/df) from the undulator output;
2. Develop a model of THz beams on the initial aperture (undulator output);
3. Model a spatial output radiation module at a central frequency of 2.889 (THz) for convenience;
4. Build a WDF to represent EM radiation in terms of GO rays (and build the LF);
5. Analyze significant LF data on the waveguide output (with desired resolution of selected coordinates);
6. Evaluate the results using the current method against previous studies that used classical methods (Gaussian, Zemax);
7. Analyze the developed models for accuracy and computational complexity.

The intended contribution of this study entails three components. The first is the development of the EM field, ultra-short THz beam models based on analytical methods, mode excitation, and decay. When only the waveguide can be replaced, or the whole undulator, the model does not change, which are the only parameters. The second is the calculation of the Wigner distribution function (WDF), the EM field representation in terms of GO rays (or LF), to allow the use of optical and quasi-optical simulations, such as the transfer matrix method and ray tracing approach, or commercial Zemax software. Third, the WDF enables analysis and diagnostics of complex beams, setting aside the fact that it allows the discovery of hidden parameters, which will directly affect the analysis and diagnostics of physical parameters of the medium, i.e., the TL components.

The remainder of the paper is structured as follows: Section 1 includes the description of the problems and our need, THz area, profit, contributions and limitations, and novel FEL construction; Section 2 presents the gap and general approach, an overview of the methods for EM field propagation analysis and calculations, and analytical and numerical simulation, which were built in commercial software. Section 3 presents the preliminary results, showing the complexity and uniqueness of the signals, along with a quantitative value, includes the results of the models for the spectral analysis. In fact, it is an explanation and preparation for using the method that will be explained in the next section; Section 4 includes the methodology, which is a brief description of the methods investigated in the research, WDF, LF [10], and GO rays representation, also, includes the results of the models and the brief spectral analysis; Section 5 presents the discussion on prospective uses of the approach, spatial characterization of radiation, and limitations; Section 6 presents the general discussion, which describes the final results of the research; Section 7 presents the conclusion, which describes the outcomes, and the impact of the research.

The main purpose of this work is to develop a tool for analyzing and characterizing general radiation for the free-electron laser (FEL) system under construction, with an emphasis on transmission line (TL) design, which is in the final design process. This will be achieved by 3D visualization and imaging of complex EM fields, which can provide 3D diagnostics for recalculating the early planning for the TL of the super-radiant THz FEL at the Schlesinger Center, Ariel University [11]. This is a shared project of UCLA and Ariel University. An electron gun was built at UCLA and commissioned at Ariel University as part of an ongoing collaboration between the two universities [12]. Other components of the FEL were designed, developed, and built at the Schlesinger Accelerator Center. The uniqueness is expressed in a new-generation design that provides a radically simpler approach to RF feeding of a novel hybrid photo injector. The hybrid gun is composed

of a standing wave section (3.5 cells) and a traveling wave section (9 cells) in a single structure; therefore, it has a much larger inner surface than a typical 1.5-cell electron gun. Such construction allows better performance in beam parameters, providing a high-quality electron beam with an energy of 6.5 MeV, emittance of approximately 3 μm , and a pulse duration of 150 fs of up to 1 nC per pulse. The FEL will operate in a super-radiance regime via the novel unique e-gun, which will produce the THz pulse. Studies in the super-radiance regime requires extraordinary beam properties. The photo-injector is an rf-LINAC gun that produces ultra-short (picosecond or sub-picosecond scale) electron beam pulses with a controlled energy chirp (driven by the FEL). At the output of the waveguide, it will radiate THz pulses. This study concentrates on a 7.5 mm \times 5 mm flat aperture simulation. Figure 1 shows a general scheme of the THz FEL. The frequency spread of the THz radiation is 10% around the resonant frequency. Due to safety restrictions, the THz radiation source is placed in an underground bunker. The TL passes the radiation to the users' rooms, with the geometry determined by the constraints of the building structure designed before this research began. Due to the high absorption of THz radiation by humidity in the air, the TL should be placed in a cylindrical plastic/metal pipe 30 cm in diameter under proper vacuum-enabling conditions to reduce losses, as shown in Figure 2.

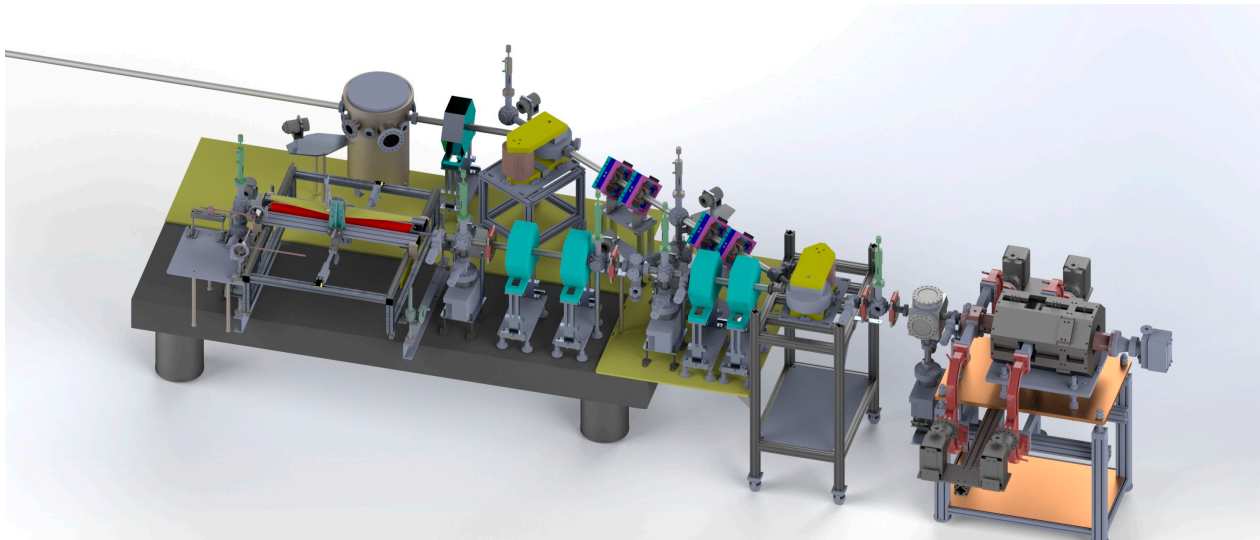


Figure 1. THz FEL setup at the Schlesinger Center.

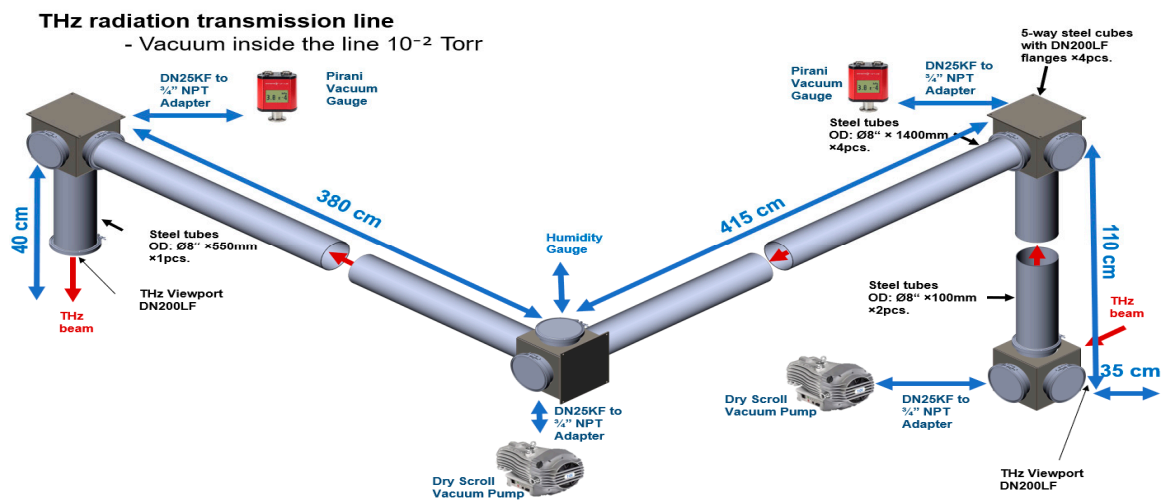


Figure 2. THz transmission line.

The TL consists of four sections perpendicular to each other. Confocal mirrors with a 90° reflection angle are installed at each junction of the central ray. Therefore, all mirrors have a common focal plane. Mirror no. 3 is not typical (even among mirrors with defined geometry, such as parabolic, spherical, etc.) in terms of the focal length. That is why its price is extremely high. This is the reason why many studies are now conducted on this topic, particularly with an emphasis on mirrors for THz. Another reason is that real radiation has a very broad spectrum. Specifics of the signals, such as an energy spectral density distribution (dW/df) of the complex beam is shown in Figure 3, explained in detail in Section 3. In addition, we are planning for an FEL system that will work in the 1–4 THz frequency range. Even in such a medium, the properties of the radiation change significantly, with an emphasis on diffraction. (Without going into detail, it is worth noting that first, energy at a frequency of 1 THz will be lost on the sides in this configuration, thus there is a need for mirrors with a larger diameter.) This means that even for the same pulse, different TLs with different parameters are needed because the shape of each beam will change drastically, even at near frequencies, as shown in Figures 4–9. In addition, even at the same frequency, the shape of the Ex beam (Figure 10a) is completely different from that of the Ey beam (Figure 10b). This means that the energy distribution is completely different, which presents challenges for the entire TL in general and the mirrors in particular. Therefore, according to the initial estimates, it is clear that there is a need for different mirrors for 1 THz and 4 THz. It should be emphasized that, even for the same profile (pulse shape), different TLs with different parameters are needed. In order to accurately plan the mirrors, it is necessary to perform a calculation for the entire shape of the pulse and match it with a mirror. Then, we can optimize the mirror for a variety of radiation profiles. The components of the fields used for this purpose are shown in Figures 4–9.

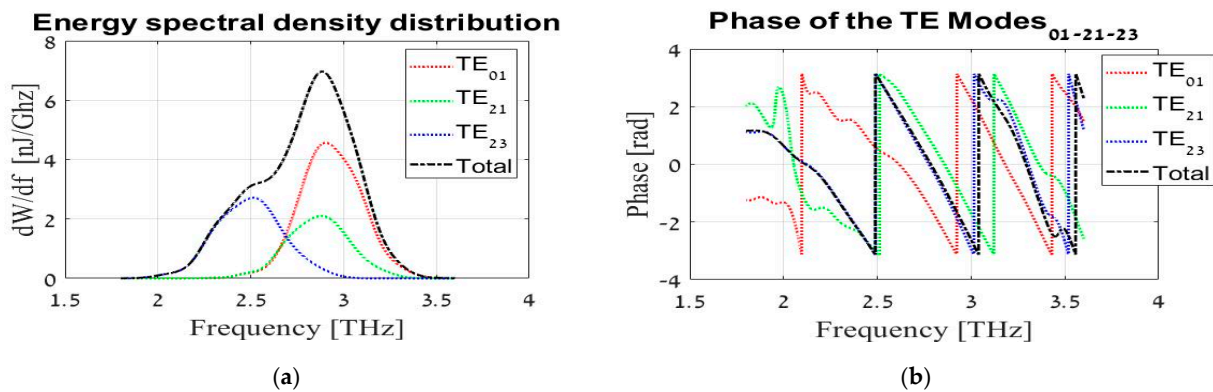


Figure 3. Output amplitude radiation spectrum of Israeli free-electron THz source: (a) energy spectral density distribution (dW/df); (b) phase.

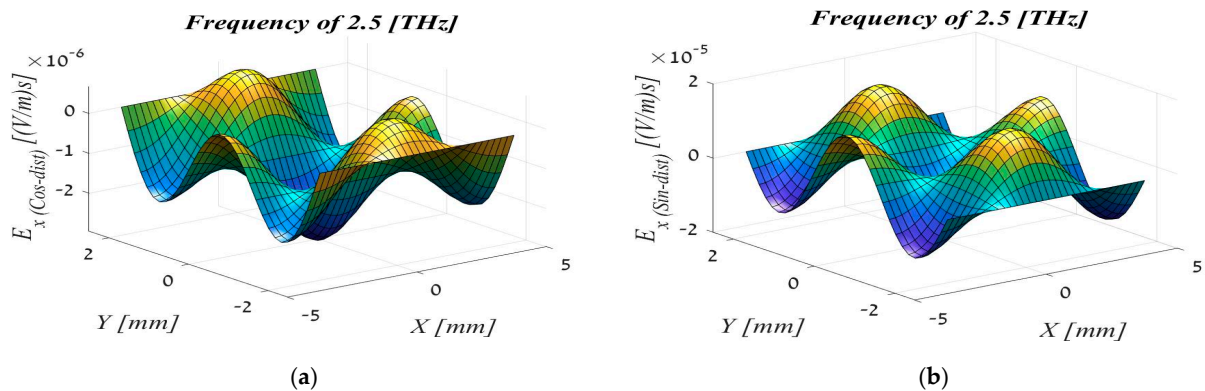


Figure 4. Spatial profile of output radiation Ex complex beam at 2.5 THz: (a) Ex cosine distribution; (b) Ex sine distribution on waveguide output.

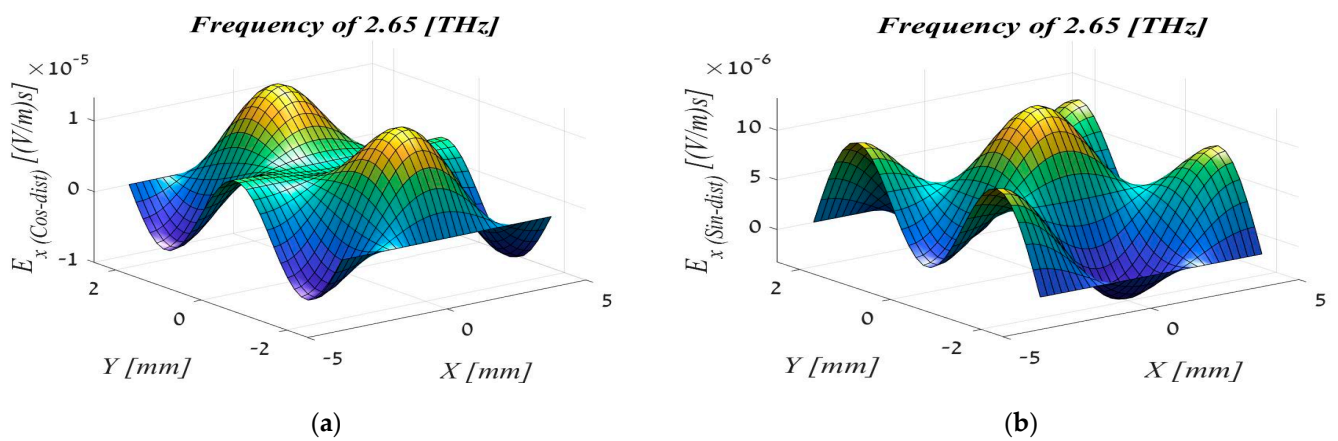


Figure 5. Spatial profile of output radiation E_x complex beam at 2.65 THz: (a) E_x cosine distribution; (b) E_x sine distribution on waveguide output.

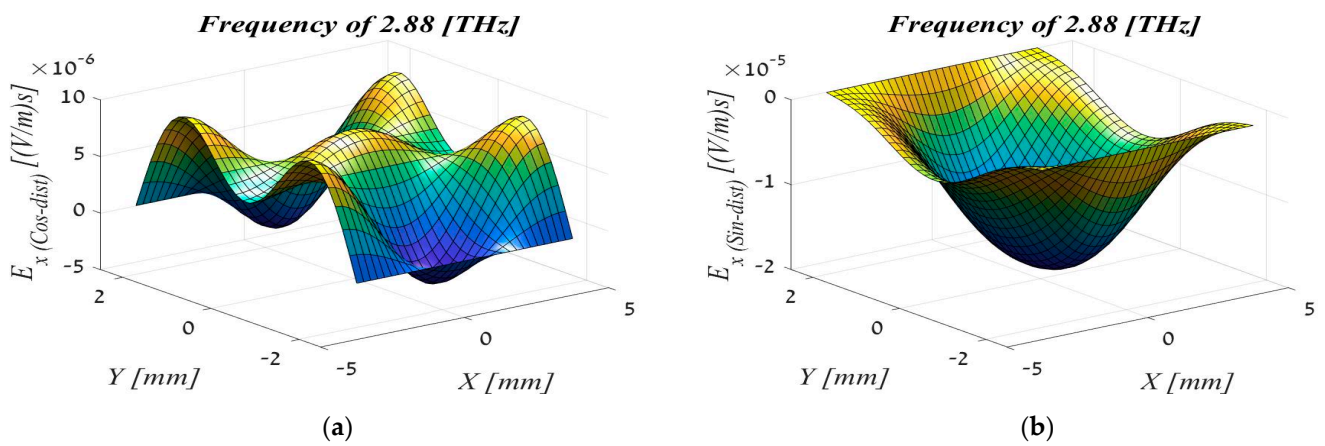


Figure 6. Spatial profile of output radiation E_x complex beam at 2.889 THz: (a) E_x cosine distribution; (b) E_x sine distribution on waveguide output.

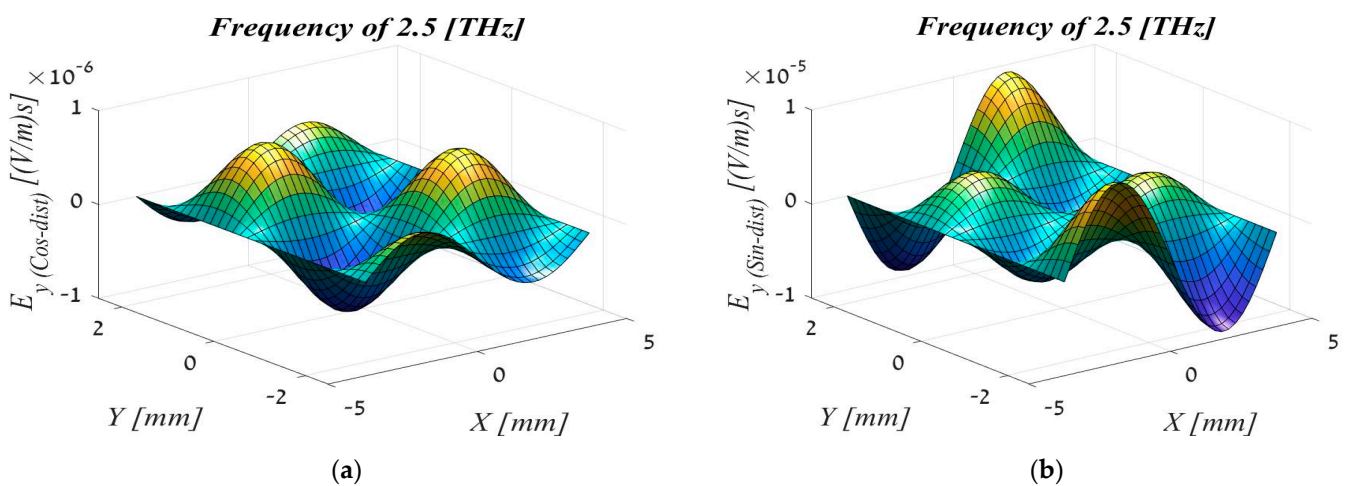


Figure 7. Spatial profile of output radiation E_y complex beam at 2.5 THz: (a) E_y cosine distribution; (b) E_y sine distribution on waveguide output.

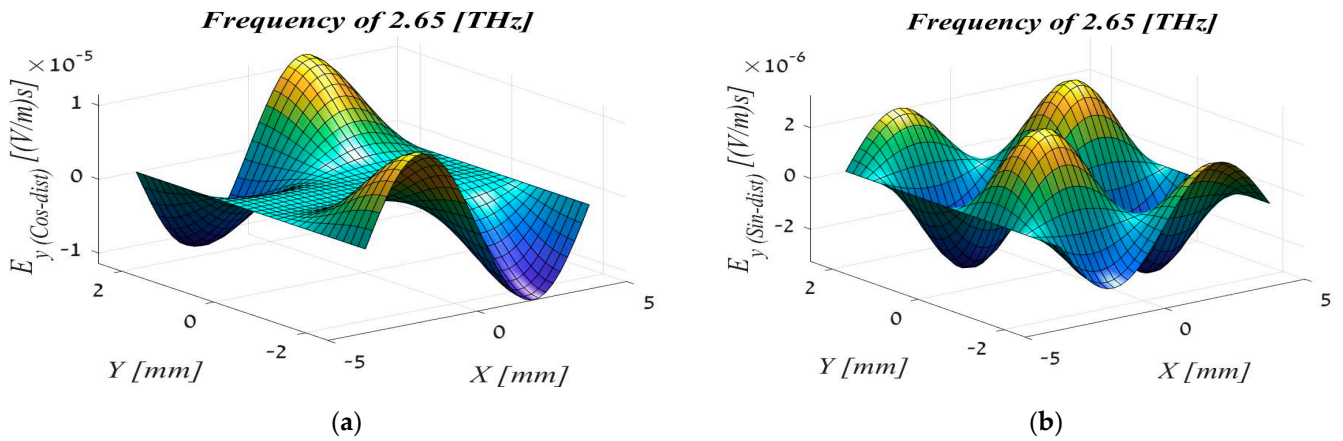


Figure 8. Spatial profile of output radiation E_y complex beam at 2.65 THz: (a) E_y cosine distribution; (b) E_y sine distribution on waveguide output.

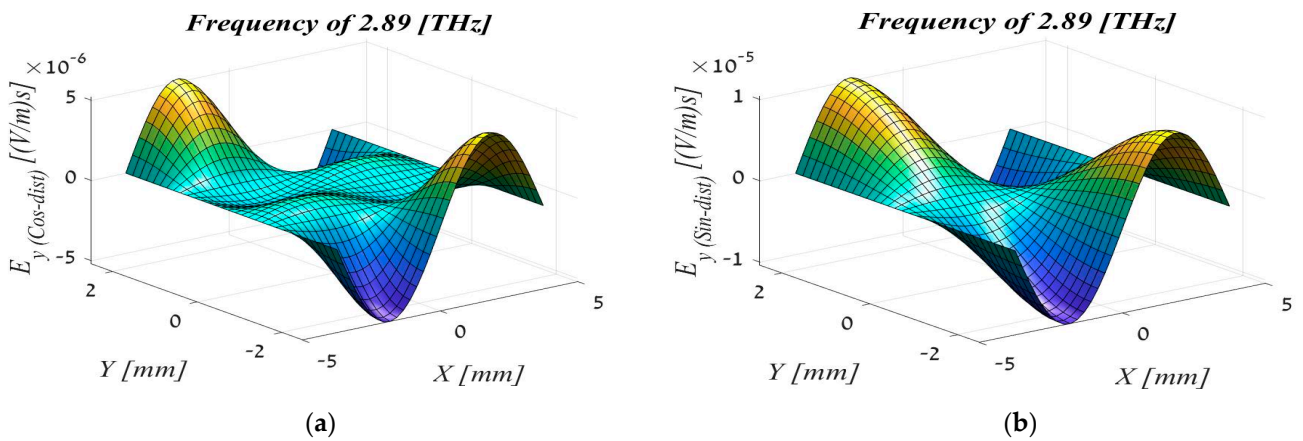


Figure 9. Spatial profile of output radiation E_y complex beam at 2.89 THz: (a) E_y cosine distribution, (b) E_y sine distribution on waveguide output.

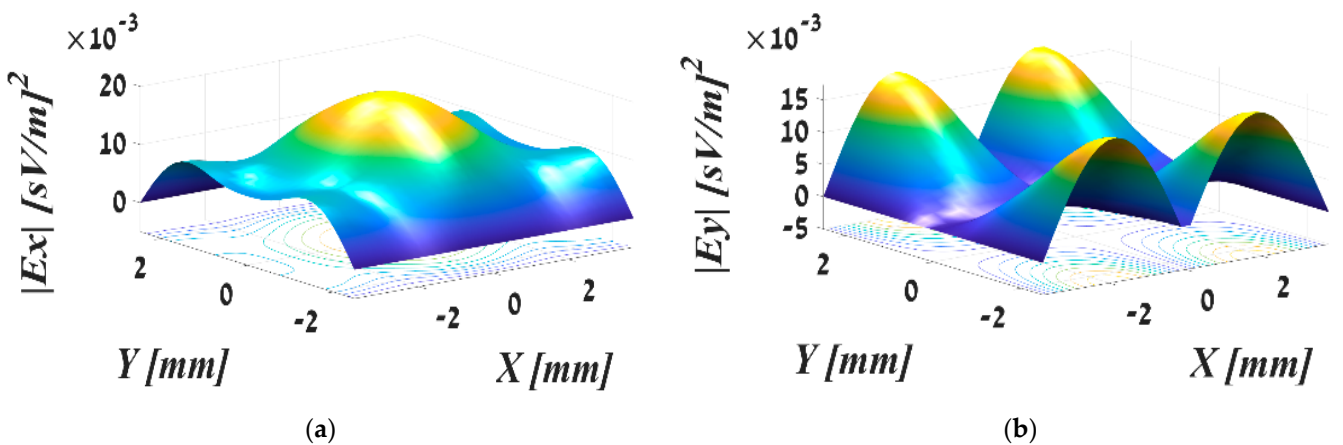


Figure 10. The module of spatial output radiation at a central frequency of 2.89 THz: (a) $|E_x|$; (b) $|E_y|$.

By default, Gaussian pulses are considered in most cases. Such a profile or shape is very convenient for scientists for a number of well-known reasons. It is also easy to follow the propagation of these pulses as well as how they spread or expand. The Gaussian pulse, or one with a similar normal distribution, correlates well with mirrors with mathematical

geometry, such as parabola, ellipse, and spheroid. A certain caustic is created around the focus point, which makes it easy and convenient to calculate and work with. In practice, the pulses are not Gaussian at all [13]. Therefore, there is a need to accurately characterize the beam in order to design the appropriate mirrors for maximum energy transfer. This is the main reason why we need to analyze and characterize the radiation. Additional support will be provided showing that the simulations are necessary for the further design of the TL.

The basic TL consists of two pairs of mirrors: a telescopic pair and a microscopic pair. There are other elements that are less important to this work. The scattering of the THz beam is quite large in relation to the visible light rays and the laser beam. It depends on the frequency (mode number and initial aperture distribution), but let us assume that its waist doubles every several inches [14]. Therefore, it is necessary to focus on each beam at the beginning of the TL. This is the role of the first mirror. That is why the shape of the beam is extremely important (and the visualization in 3D). Another reason is that the general research (including research in various departments) deals with the construction of a smart TL using an AI approach, which learns the range of pulses and optimizes the mirrors for the purpose of transmitting radiation most efficiently at the main working frequency for the transmission of optimal radiation at a variety of frequencies. This work instead deals with characterizing the energy distribution for the purpose of general study.

The previous TL design was based on parabolic mirrors, considering solely the E_x part of the $E(E_x, E_y)$ complex EM field. E_x itself is a complex beam transmitted as an ultra-narrow pulse, which is a rather complicated matter because the beams (real and imaginary parts of E_x) also change over time. Therefore, the design was performed according to the absolute value of the E_x complex beam when it is at maximum amplitude. This function is approximately reminiscent of a particular Gaussian beam (Figure 10a). Therefore, parabolic mirrors were chosen. This is how the TL is actually planned and built in most cases. This approach allows for precise planning, considering all the parameters. In addition, for the first time, a complex E_y beam was explored as a preliminary result specifically for this work, while the emphasis in this study is on the 3D characterization of the entire EM field and analyzing all of its components separately.

As long as the accelerator is under construction and the TL is in the design stage, it is not possible to conduct experiments, so this is another reason for developing a quality simulation. Experiments can be carried out in similar systems for the purpose of justifying a later method, such as a diagnostic method for THz pulses produced by EA-FEL [13].

2. The Gap and General Approach

2.1. Review of Simulation Methods

The Wigner distribution function (WDF) is one of the methods used for analyzing radiation and its propagation, which not many researchers commonly use, as few of them know it well. Most researchers prefer classical methods, such as solving the Maxwell equation with various computational accelerations. This requires them to reduce the resolution due to an endless demand for resources such as memory and computing power. Most physicists see problems in the techniques they have learned, and as a solution, they approach ready-made “solvers” in the hope that they will give them the best answer. This is understandable because they do not have engineering evidence and algorithmic tools. Therefore, in order to solve complicated numerical problems, commercial software is used, such as CST, HFSS, FDTD, and Zemax (Zx), even when these methods provide a limited solution and do not meet all the parameters. For this type of problem, CST is not effective at all; it has no built-in solvers and is simply not designed for this type of task. Except for Zx, these electrodynamic solvers require that the boundary conditions be defined. In fact, their solution is aimed at modeling compact structures that have an energy flow in arbitrary directions of the Maxwell equations. Due to the short wavelength, the grids become prohibitively large and require extensive power and memory. Each dimension requires at least 10 space samples per wavelength. Concretely, the space mesh cell size

(Δr) is about 10 μm . The ratio of time-step size (Δt) correlated with the space mesh cell size has the relationship $\Delta r \gg C_0 \Delta t$, where C_0 is the speed of light in a vacuum. Thus, such a solution requires about 10^{17} space mesh points and 10^6 time steps for each EM field component. Hence, FDTD functions quickly in the THz area. In addition, a large number of mesh elements and samples must be used, which increases the accumulated computation errors.

Zx is suitable but with strict restrictions, and the input data must be in the form of GO rays, which was the case in this work, and when we already have the EM field representation in the rays, then Zx is no longer useful. In addition, in order to set lenses or mirrors, the dimensions of Gaussian parameters such as maximal angle must be supplied. This is repeatedly an approximation to a Gaussian beam. The effect of each mode on the TL was calculated separately and analyzed and representation in Zx was carried out in [14]. Working with Zx is very complicated and always requires a researcher familiar with it. In addition, there is a constant need to be in touch with technical support. Besides the limitations of the software, dedicated requirements, and approximations of the data, the license is very expensive, and this is why our center and all of the universities in our country have stopped working with it. Therefore, in this study, all the simulations (and their algorithms) were designed from scratch. The pulses are at the THz frequency, which requires enormous resources, and therefore, the known methods and techniques that were not suitable for this work were rejected, including the techniques discussed in [15]. In our previous work, the TL was investigated with Hermit Gaussian (HG) modes [16]. The study was performed by estimating the important parameters of the TL and the radiation that emerges in users' rooms [17]. This was a fairly thorough study, under limitations that we overcame in the present work. In the previous work, spacial profiles of the output radiation field components with the same characteristic frequency points were considered only for the Ex beam module. Also, the TL model was simplified to the on-axis and central axis when the mirrors were approximated with thin lenses. The most important factor was that the previous work used Gaussian beam mode analysis to describe the propagation of the wave packet emitted from the waveguide. The evolution of the Gaussian beam parameters in free space and the optical elements were described by using ABCD matrices [18]. Implementing this technique in c++ code enabled us to demonstrate the energy distribution pattern of a multi-mode EM beam in different transverse planes along the TL. This has a great significance in the design of optical elements along the TL (by fitting them with dimensions corresponding to the EM beam), and understanding the consequences of the TL diameter on the energy loss pursuant to beam divergence. Using the methods considered and implemented in this research, the field pattern and beam width in front of the optical elements along the TL were estimated, as well as the energy flux distribution spectrum for the wave packet under concern and the TL. Actually, this is a favorite numerical calculation method among many researchers [19]. The method is quite convenient but fixed in hard limits under non-negligible approximations. It must be noted that the most prominent disadvantage here is that the method works only for paraxial approximation for very small angles. An important conclusion was obtained from this research, which reinforces the use of the method proposed in the current work.

Most studies that use the WDF emphasize field representation in the time–frequency domain (of transformation), whereas in this study the emphasis is on the spatial–frequency (phase space) domain, with time–frequency as an additional option in order to estimate the field expansion in space. In addition, most studies address one dimension of the WDF, probably due to its complexity. In this study, we present a 3D analysis of the space–frequency and time–frequency domains.

In addition, as already mentioned, this work constitutes a basis for calculating radiation transfer in the most efficient way in future research when the planning techniques applied are ML methods. In other words, some non-trivial pulses should be transmitted in the most efficient way through the TL. That means, without changing the pulse and losing its power (energy), the medium should be changed in such a way that allows the

pulse to pass in the most efficient manner. It is clear that each pulse will require a different change of medium; therefore, there will be some optimization of the range of pulses and frequencies. The second goal is to perform the field transformation from the shape of some function to the desired Gaussian. That is, it is a mode conversion. Therefore, the classical and other known methods cannot provide any answer to our challenge. Hence, the WDF was chosen.

2.2. Research Purpose

In addition to what was mentioned earlier, the technical aspects are emphasized here. The goal was to characterize the radiation profile of wideband ultra-short THz beams. As stated, each component of the EM field (E_x and E_y) is complex. Therefore, the pulse will be represented by four components (real and image amplitude for E_x and E_y , respectively) for each individual frequency. This is intended for future calculation of the smart mirrors that will transmit the pulse most effectively. This simulation is an integral part of the overall system design. Assume that the beam is pure Gaussian. Therefore, a mirror (let us say the first one in the current TL) that has a suitably defined geometry (as mentioned in the Introduction) will focus the beam in a certain caustic around the focal point. Even without going into non-linear effects, such as aberrations (for which a pair of confocal parabolic mirrors cancel the second order, and we have exactly two such pairs), under conditions of perfect geometry, when the beam is also defined in a precise mathematical way, the TL can be studied by HG modes [17]. Indeed, mathematical answers that line up nicely are achieved for the planning of the TL in general and mirrors in particular. This is a classic method, well accepted in the field, which we have carried out this research [17].

Obviously, HG decomposition is an approximation, if at all possible, and therefore it introduces an additional error when unsatisfactory results are obtained under ideal conditions, and all this is under paraxial approximation only. This approximation was made for a real part of the E_x field only, or its modulus. In reality, the beams are not Gaussian. The profiles are completely different from pulse to pulse, even for the same field at the same frequency at the same time (the E_x beam is completely different from the E_y beam), as shown in Figures 3–9, and even their absolute value (Figure 10), the shapes of the pulses, that is to say, the profile functions, are not completely Gaussian. Therefore, the most appropriate method in this case is the WDF. The beam's components are orthogonal and therefore can be separated for calculation. As noted in the Introduction, THz radiation has properties of both millimeter waves and visible light. Therefore, diffraction is very high, and it is necessary to focus the beam along the TL trajectory. The WDF allows the field to be represented as a set of GO rays when diffraction is considered. It can be seen that the EM field transmission by the GO rays leads to excellent results for frequencies 10 and 100 times lower [20] (also published as GJM [21]), which are known to have significantly higher diffraction than in this study. In addition, this experimental study shows that it is possible to reduce the scale and work with a small model of the tunnels. The results show excellent correlation both with the scaling change and in comparing simulations with real experiments in tunnels. In fact, this exactly fits the design of the TL. The mirror design was explained to justify this work as a simulation for a general purpose.

The main goal was to design a TL to transfer radiation in the most efficient way. Hence, the shape of the mirror and its profile function must also change according to the functional components of the beam. This work provides a spectral analysis of all components of the field, for each frequency and mode that make up the beam. Another advantage of this work is that all of the parameters can be changed, so this simulation is a broad platform for the analysis, characterization, and diagnostics of radiation. At the same time, an LF is obtained, which can form the basis of input data for work with the RT technique in any software, input data for AI systems, or input data in Zx format or other commercial simulations in optics and quasi-optics. This is another reason for choosing the WDF.

3. Preliminary Simulation Results

3.1. FEL Simulations of WB3D as Pre-Results for This Work

As a result of the WB3D simulation, three main modes were obtained in which most of the energy was concentrated. These are waveguide modes TE01, TE21, and TE23, which are mainly excited by the electron beam. (In the real world, the exact model includes more modes, with lower energy contribution by several orders. Hence, the model with three modes was accepted.)

A hybrid laser-driven photo-injector was used to produce very short energy-chirped relativistic electron bunches. The enhanced super-radiation mechanism enabled the effective production of strong pulses of THz radiation [22]. The WB3D simulation was supposed to utilize those electron beams for radiation excitation and beam propagation analysis (in the source) [23]. This approach is based on a self-consistent, space–frequency description of the propagation of a pulsed relativistic electron beam through a magnetostatic structure and its radiation emission [23]. The simulation has been successfully applied for the analysis of various processes taking place in free-electron radiation sources (see [22] and references therein). The numerical WB3D code for radiation pulse simulation at the output of the Israeli THz free-electron radiation source was developed from scratch at Ariel University.

According to this analysis, the power is concentrated in the three modes mentioned above. The maximum power is obtained at three frequencies: 2.889 THz (peak of TE01 and TE21 components), 2.5 THz (peak of TE23 component), and 2.65 THz (intermediate point where all components considered to have approximately equal spectral energy flux), as can be seen in the radiation spectrum in Figure 3a.

The energy spectral density distribution (dW/df) of the beam is shown in Figure 3a and the phase is shown in Figure 3b. The TL is designed according to these characteristics. The dominant waveguide component indicates the beam shape corresponds to the symmetry at a chosen characteristic frequency. Following that, the output beam function keeps the boundary conditions at the walls of the rectangular waveguide in which it is excited.

The phase is very important in the EM complex field, especially when each component of the field is itself complex. It can even be said to be critical because it actually determines the energetic information (energy distribution) at every point in space. It is, therefore, very important to maintain the phase accumulation in the mirror damage accurately. As is well known regarding free passage in the medium, polarization varies like any component at the point of impact in the mirror. In this regard, it is very important to characterize the complex EM field by its components at the exit point from the waveguide. This work characterizes, compares, and explains this point.

3.2. $E(E_x, E_y)$ EM Complex Field Presentation

Since this work is intended to complete all the corners in terms of their fields and variations, the emphasis here is placed on the 3D characterization of the field component that changes over time. Figures 4–9 show spatial profiles of the output radiation of complex fields E (E_x, E_y) at the most important points of the frequencies. The three impact frequencies of 2.889, 2.5, and 2.65 THz are where the radiation is at high power. Figures 4a, 5a and 6a show the mean E_x cosine distribution, the real part of each E_x beam at those frequencies. Figures 4b, 5b and 6b show the same important points, with only the imaginary part or sine distribution of the E_x beam in the same points. Figures 7a, 8a and 9a show the real part of the E_y complex beam, and Figures 7b, 8b and 9b show the imaginary part of the E_y beam at the important points.

As can be easily seen, the beams have completely different energy distribution from each other, even between the nearest frequencies (Figure 3), where most of the energy is transmitted (Figures 4–9). But even at the same frequency, the real parts of the E_x beam components are completely different from the real parts of the E_y beam components (Figures 4–6 and Figures 7–9, respectively). Even the pulse components themselves are different from each other (Figures 4–9). This is, therefore, not a trivial problem, especially at

THz frequencies with ultra-short beams, which is why so far, all the designs have referred to the Ex field only.

3.3. A Module Representation of $E(E_x, E_y)$ Complex EM Field

Humans can distinguish only three dimensions; therefore, as much important information as possible will be present in each figure. A module of the Ex and Ey beams at the resonant frequency with the highest energy distribution is presented here, which also constitutes a complex EM field, and the LF [24] with the emphasis will be displayed on it. Hence, the main planning of the TL is around that frequency. For the analysis, calculation, and design of the TL, a representation of rays is made for each complex beam separately. This means that only the intensity of the radiation will be displayed, when in fact the amplitude is complex. The intensity allows us to estimate the power and also decide on the physical properties required for the mirror. In fact, it is enough to know the absolute size and intensity of each beam and its direction in space in order to design the desired system. When the complex amplitude carries within it information about the phase of time, it indicates how the EM field changes over time. It is important to disregard it in order to accumulate phases when assembling the EM field somewhere in free space. Either way, it is easier to explain to the average reader when it comes to the absolute value.

Figure 1 shows Ex and Ey at a frequency of 2.889 THz (perpendicular to each other). This is actually a resonant frequency of the system, which also indicates the absolute synchronization of the electron beam. Thus, a symmetrical shape is obtained when most of the energy in the Ex field is concentrated in the center precisely at that moment, with energetic restraint on the part of Ey at the ripple's edges. The intensity of the beams is of the same order of magnitude and almost identical. Therefore, the Ey part of the field cannot be neglected, which the previous TL design did not consider.

4. Methodology

The WDF has long taken pride of place in the field of optics [25] and quasi-optics. It was introduced by Eugene Wigner in 1932 as a quasi-probability distribution to study quantum corrections to classical statistical mechanics [26]. The WDF plays an important role in the characterization and propagation of electromagnetic fields and is a tool for modeling optical field (linear and nonlinear beam) propagation [27]. One can see from previous publications that the analysis works for both coherent and partially coherent beams. Thus, there are current publications on this topic regarding both the paraxial and non-paraxial regimes [28].

In addition, it has become a very useful tool for the theoretical analysis of optical (including quasi-optical) systems [29,30], acoustic holography [31], signal processing [32], radar emission [33] for its characteristic representation, and radio waves used in wireless technology [34]. It has been utilized in numerous applications as well as real physical experimentation. The WDF is related to time–frequency analysis [35] in a vast majority of studies and is less applied to spatial frequencies, which are of greater importance in this work.

A general approach to complex electromagnetic (EM) fields is represented in this research, where each beam component, such as Ex and Ey fields, is also complex. In addition, the novelty here is an inexact description of free electromagnetic wave fields in terms of rays [36,37] with emphasis on THz radiation systems and spectroscopy (see [15,38] and references therein).

The WDF is a new way of characterizing EM fields, especially as a unified description of partially coherent beams when exploring the concept of phase space. Following Alieva et al. [39,40], evaluation intensity, phase coherence, beam width, and other beam parameters during propagation can be described by the pure space or the pure spatial–frequency representation of a stochastic process via its mutual intensity (MI).

MI is a function of four variables in Equation (1), where r_1 and r_2 are vectors. It describes the beam behavior, where the brackets are used for time or spatial averaging and

the asterisk (*) indicates a complex conjugate. The intensity distribution $I(r)$ corresponds to a square module in Equation (2). This parameter can be measured.

$$\Gamma(r_1, r_2) = \langle f(r_1) f^*(r_2) \rangle \tag{1}$$

$$\Gamma(r, r) = \langle |f(r)|^2 \rangle \tag{2}$$

The WDF of an EM field, $W(r, p)$, is defined by its MI, represented in Equation (1). It can also be described in terms of its directional spectrum, as represented by Equation (2) and its equals (according to [39,40]).

Therefore, it is easy to explain the “ray concept” in the GO by this space–frequency description. In ray optics, each ray is defined by its position and direction. Hence, the WDF of each beam, $W(r, p)$, is the amplitude (3, 4) where the ray passes through point r with frequency p (i.e., direction q).

$$W(r, p) = \int \Gamma\left(r + \frac{\tilde{r}}{2}, r - \frac{\tilde{r}}{2}\right) e^{(-i2\pi p\tilde{r})} d\tilde{r} \tag{3}$$

$$W(r, p) = \int \bar{\Gamma}\left(p + \frac{\tilde{p}}{2}, p - \frac{\tilde{p}}{2}\right) e^{(+i2\pi r\tilde{p})} d\tilde{p} \tag{4}$$

A set of GO rays defined by the WDF represents the EM beam propagation in space [41]. Let us define a flat aperture as the initial position of that ray’s set; in the real world, this flat aperture is the waveguide’s output. The WDF of the beam is perpendicular to the z -axis in an ideal case. To simplify the explanation, let us concentrate on a known monochromatic field distribution on the aperture. In this simple case, the WDF of a total complex $E(x, y)$ field in terms of rays can be defined for each component separately, and this also helps to simplify the task because the E_x complex field is orthogonal to E_y .

Therefore, the WDF of the E_x can be defined as follows:

$$\begin{aligned} &W_x(x, y, k_x, k_y) \Big|_{z_{aperture}} \\ &= \int \int E_x\left(x - \frac{\tilde{x}}{2}, y - \frac{\tilde{y}}{2}\right) \Big|_{z_{aperture}} \cdot E_x\left(x + \frac{\tilde{x}}{2}, y + \frac{\tilde{y}}{2}\right) \Big|_{z_{aperture}} \cdot e^{(+ik_x\tilde{x})} \\ &\quad \cdot e^{(+ik_y\tilde{y})} d\tilde{x}d\tilde{y} \end{aligned} \tag{5}$$

The WDF of the E_y can be defined as follows:

$$\begin{aligned} &W_x(x, y, k_x, k_y) \Big|_{z_{aperture}} \\ &= \int \int E_y\left(x - \frac{\tilde{x}}{2}, y - \frac{\tilde{y}}{2}\right) \Big|_{z_{aperture}} \cdot E_y\left(x + \frac{\tilde{x}}{2}, y + \frac{\tilde{y}}{2}\right) \Big|_{z_{aperture}} \cdot e^{(+ik_x\tilde{x})} \\ &\quad \cdot e^{(+ik_y\tilde{y})} d\tilde{x}d\tilde{y} \end{aligned} \tag{6}$$

Coordinates (x, y) are the physical points on the aperture (waveguide output). The space angles (k_x, k_y) are conjugated variables of a Fourier transform in the space coordinates. When the time dependence of the EM field transfers is considered, the dimension of the WDF increases from 4D to 6D.

As a result, the rays from each point xy on the aperture are obtained. The direction of each ray is defined by the wave number $k = (k_x, k_y, k_z)$, where

$$k_z = \sqrt{\left(\frac{\omega}{c}\right)^2 - k_x^2 - k_y^2} \tag{7}$$

The complex ray amplitude and polarization (I) are defined by the WDF as

$$I_x(x, y, k_x, k_y) = W_x(x, y, k_x, k_y) \tag{8}$$

$$I_y(x, y, k_x, k_y) = W_y(x, y, k_x, k_y) \quad (9)$$

The complex ray amplitude I_z is obtained due to the orthogonality in any uniform media of the ray polarization to the ray wavenumber ($I \perp k$).

$$I_z = \begin{cases} -\frac{I_x \cdot k_x + I_y \cdot k_y}{k_z} & k_z \neq 0 \\ 0 & k_z = 0 \end{cases} \quad (10)$$

Thus, for each given beam distribution (E), the set of rays $I(x, y, k_x, k_y)$ is obtained for each physical point (x, y) on the aperture. The E_x and E_y beam propagation in space is represented by the propagation of the GO rays [41]. All equations represent a single-frequency problem. For multiple-frequency problems, we follow all steps mentioned above for each frequency separately.

5. Results

WDF Simulations

The vast majority of studies that use the WDF focus on its time domain is 1D. In this study, the 3D spatial domain is important in order to diagnose the form of energy distribution for each beam, as well as the beam's propagation. Almost all researchers have used the WDF for analytical solutions. However, no simulation was found for our needs. Therefore, a special code to implement the WDF was developed from scratch for this study purpose. For each coordinate in space an LF is obtained, a pulse consisting of rays at all kinds of angles. The number of rays and representation of angles can be controlled according to the need and convenience, depending on the resolution of the aperture (which depends on the initial sampling resolution).

As can be seen from Equations (5) and (6), for a simple two-dimensional field, a 4D WDF is obtained. The complex amplitude adds an additional dimension. The XY physical coordinates mark the initial beam position on the aperture. K_x and K_y are spatial angles relative to the Z-axis. The beam is not static and it changes over time; therefore, another dimension is added. These changes are harmonic and behave according to sine and cosine. The LF in the center of the aperture (coordinates $X = 0$ and $Y = 0$) is shown in Figure 11. Figure 11a shows the WDF from the E_x beam and Figure 11b shows the WDF of the E_y beam. The figure shows the total of rays in all directions emerging from the midpoint (center) of the waveguide. In I_x , the angle spread of K_x and K_y is very small and thus is negligible in the energy dispersion. It can be concluded that the radiation is focused and directed exactly parallel to the Z-axis, without unnecessary deviations, and the energy is mostly concentrated in the center. In the E_x beam, the first mode is dominant, thus the shape of the field is reminiscent of the normal distribution in the middle. When most of the intensity is concentrated in the middle of the field it is uniform, thus in the representation of the rays, a uniform concentration is also seen in the middle. Therefore, paraxial approximation can work in this case and can indeed be simplified with Gaussian beams.

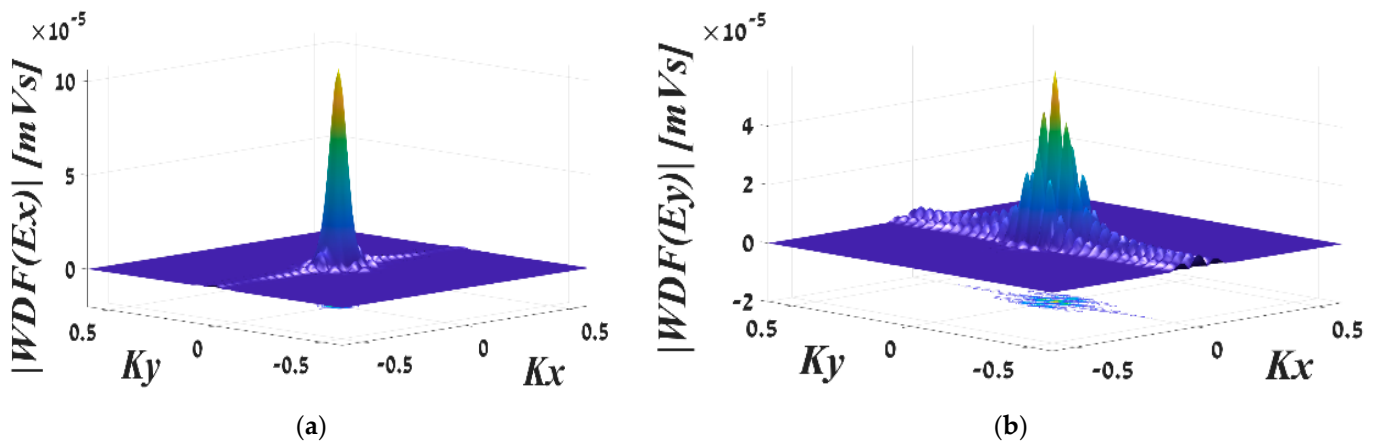


Figure 11. Ray intensity in aperture center, W_x ($X = 0, Y = 0$), at a central frequency of 2.889 THz: (a) I_x ; (b) I_y .

Figure 11b shows the E_y field representation, where 12 concentrations of different transmission angles can be seen. These are the most important 12 directions, but their scattering is not large and is concentrated around zero. That is, the significant transmission direction is parallel to the Z-axis. This is because the energetic distribution of the E_y beam is uneven on the aperture, consisting of four peaks. It can be concluded that the dominant mode at the resonant frequency is mode TE_{21} .

A type of ripple can also be noticed. In Figure 11a, the ripple is almost negligible, which means that from the center point, there is almost no transmission of rays at large angles relative to the Z-axis. In Figure 11b, a more significant ripple can be found, which indicates that there is energy at the edges. But here, too, the transmission concentration is along the Z-axis. This is less important in this study, but what stands out is the direction of the ripple. In Figure 11a, it is along the X-axis, while in Figure 11b it is along the Y-axis, which reinforces the correctness of the result obtained. The directions of the ripple vary with respect to the direction from which it reached the center of the aperture, but what is saved is the attitude. The ripple that appears in I_x is perpendicular to the ripple in I_y .

Figure 12 shows the entire aperture containing all the rays emanating parallel to the Z-axis from each defined coordinate ($K_x = 0, K_y = 0$). It is worth noting that these rays have the highest intensity because of the original transmission direction along the Z-axis. Therefore, it can be seen that almost all the energy is concentrated in these rays. Figure 12a shows the normal distribution reminiscent of Gaussian, which makes sense considering the shape of the E_x field. This is further confirmation that a paraxial approximation can work in this case and it is indeed possible to simplify with Gaussian beams.

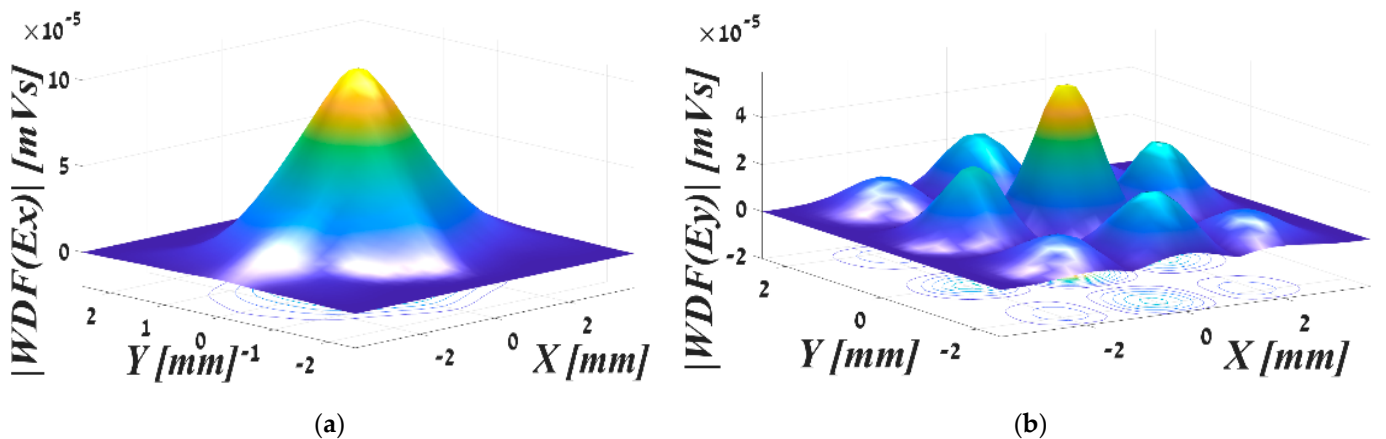


Figure 12. Ray Intensity the entire aperture, only with rays propagating parallel to the Z axis (a) W_x ($K_x = 0, K_y = 0$), (b) W_y ($K_x = 0, K_y = 0$) of the radiation field at 2.88 [THz].

Figure 12b shows the special and non-uniform distribution. It is found that the rays emitted parallel to the Z-axis do not constitute a uniform energy distribution. These are eight main equal distributions, with the main transmission direction being along the Z-axis. In addition, we can see the level in the middle, which indicates the level of radiation at $K_x, K_y = 0$.

In fact, this is the most significant information describing the behavior of the beam for the purpose of this study.

6. Discussion

This work presents the spatial profile of output radiation for a complex EM field, where all of its components are complex beams and the entire beam component is transmitted as an ultra-narrow pulse. The results were obtained as expected and with the desired resolution. It is worth noting that Figures 10–12 were constructed after interpolating the representation in Matlab for better understanding.

Figure 12a shows the normal distribution reminiscent of Gaussian. As mentioned, the propagation direction is along the Z-axis. Therefore, the pulse that advances parallel to the Z-axis behaves like a Gaussian beam and carries most of the energy. Therefore, if only parallel rays were translated, this would mean the transmission direction is precisely aimed, and there would be no need for a smart mirror. Also, the initial design of the TL with parabolic mirrors is quite correct. But the wisdom is to transmit the radiation in the most efficient way. It can be concluded that this is the desired distribution in the final stage of the target.

It can be seen that the intensity of these rays is also very high compared to the rays that are emitted in different directions relative to the Z-axis. It can be clearly seen that the larger the angle of the Z-axis, the lower the intensity. This is consistent with the theory and is pointing such that most of the radiation will propagate parallel to the Z-axis, as planned.

Figure 12b shows I_y . At first glance, it might seem that something here is not understood. When representing the intensity of the E_y beam in Figure 10b, there is no amplitude in the middle of the aperture, whereas Figure 12b shows all the rays that were emitted in parallel from the entire aperture space. A logical question arises as to where the radiation came from or whether something is wrong with the simulator.

In each case, we tackled the problem, despite the challenging obstacles. Finally, the strongest radiation was received in the center, as shown in Figure 12b. Therefore, we performed an integration of the central point and its environment; when the integrated information is taken, it is full of complexity. The result, according to an accurate calculation, is $I_y(0, 0) = 5.6404e - 23 + 5.0770e - 23i$. It can be assumed that the answer is zero. Applying the WDF to the actual and simulated parts separately also provides a nil result.

Yet the result shown in Figure 12b is correct, as the representation, in the sense of the rays through the WDF, shows the phase space. In other words, it presents the spatial frequencies, and spatial distribution is represented here, as mentioned. This means that the phase, angle $K_x, K_y = 0$, shows us the spatial frequency 0,0. Looking at Figure 10b, we see the positive peaks around zero. We can imagine an absolute sine signal or the square of a sine (in a single cycle window). After a one-dimensional Fourier transform, with the harmonics of sine, positive and negative plus zero frequencies are obtained. This means that DC is calculated as the average of the signal. This is exactly what is seen here, just in 3D. We find that the WDF is productive on MI, as can be seen from Equations (3)–(6). This is not so trivial, especially at first glance, therefore we will explain it here.

As mentioned in the analysis of the results, Figure 11a shows the intensity of the radiation of the E_x beam, while Figure 11b shows the intensity of the E_y beam. This provides an excellent indication that the radiation is mostly advancing parallel to the Z-axis. At the same time, it is known that the WDF maintains the profile of the real beam. Therefore, when such an indication is found in the sense of the rays in terms of spatial frequencies, it can be concluded that at a frequency of 2.889 THz, there is synchronization between the electronic beams and the undulator. Further analysis of the subject goes beyond this

framework and is within the purview of researchers from another department. As also mentioned with respect to the ripple, it is perpendicular between I_x and I_y (Figure 11a vs. 11b). Because the simulator computes the beams, the desired and expected result was obtained. We can see that the absolute value of the E_y beam is indeed perpendicular to the absolute value of the E_x beam in all the images, especially their absolute values, as shown in Figure 10.

Figure 12a clearly shows that the HG mode decomposition method is not suitable for this design. More precisely, we can actually see the condition for using HG, that is, provided that the angles are very small, a paraxial approximation, as claimed in the Introduction. We have received support and justification for the WDF method, which is also shown here by the fact that in a paraxial approximation, a beam behaves approximately as a Gaussian. The exact same distribution is shown for the E_y beam in Figure 12b.

7. Conclusions

This study presents the 3D spatial profile of output radiation for non-trivial radiation, transmitted as an ultra-narrow THz pulse for the design of a TL of an innovative particle accelerator. From Figure 12 it can be concluded that a parabolic mirror, positioned parallel to the propagation axis, is approximately suitable for transferring most of the energy.

In this research, a special tool was built to handle that challenge. A unique simulator was built from scratch. The simulation provides the ability to perform 3D diagnostics for an early TL design by analyzing such special radiation. The radiation characterization can be achieved from 3D imaging of the ultra-short THz pulses and its visualization. A mirror design as part of the TL can be calculated from the LF [42], as a representation of the complex EM fields. The algorithm is adjusted for phase–amplitude and spectral characteristics of complex multimode radiation generation in a free-electron laser (FEL) operating under various operational parameters. A general EM field on the edge of the source is represented in the frequency domain in terms of cavity eigenmodes. This representation is the result of a WB3D simulation, developed to obtain an indication of the complex EM field.

A 3D space–frequency analysis was provided by the WDF to discover hidden details, in which a complex EM field is transformed into a set of geometrical optical rays. Such representation is much simpler to describe the dynamics of EM field evolution in future propagation analysis and allows us to determine an initial design for the TL. A general ray approach allows operation in linear and non-linear regimes [27].

The simulation was successfully implemented for the purpose of calculating, analyzing, and 3D diagnosing special radiation with quite extreme parameters when the accelerator itself is challenging and the process is detailed so that it no longer matters what the frequency is or how short the pulse is, at least when working with simulations, until the technology allows to detect and visualize single extra-narrow pulses in the THz region. Among the recent progress made in the THz application using classic methods for computing EM wave problems is a transfer matrix method, which simulates some mediums and transmits the rays. Our simulation is a basis for using these methods, such as the RT method, Zemax, and others.

To sum up, we received a bonus, which was an ultra-short pulse simulation of THz, which we converted to a representation in an LF. Hence, all the techniques of geometrical optics are valid. From here, we can use all the techniques of image processing, data compression and coding of the integral imaging data [43], computational imaging and parallel processing. The method is most convenient for parallel processing [44] and can be run with a GPU.

The simulator was designed with Python code from scratch, without the use of built-in functions for the special purpose of the accelerator center. The entire tool showed the correct results. When the tester encounters a complex EM field in the THz range with complex components, each component of the beam is an ultra-narrow pulse on the order of femtoseconds. All components of the EM field were calculated on a small aperture of 7.5 by 5 mm, which is a waveguide output. The E_y field is generally thought of as a precursor,

and for the first time, its full characterization in 3D was obtained in this study. The method was developed for the phase–amplitude and spectral characteristics of complex multimode radiation generation in a free-electron laser (FEL) operating under various operational parameters. The tool succeeds in diagnosing an early design of the TL of an innovative accelerator at the Schlesinger Family Center for Compact Accelerators, Radiation Sources, and Applications and can be applied to any type of TL. We are confident that our tool can present the 3D spatial profile of any kind of output radiation, represented in terms of GO rays or LF along with an in-depth 3D analysis, according to the needs of the study.

Author Contributions: Conceptualization, M.G. and A.F.; Methodology, E.D. and A.F.; Software, M.G., V.P.N. and J.G.; Validation, M.G., V.P.N. and A.F.; Formal analysis, A.H.Y. and J.G.; Investigation, M.G. and E.D.; Resources, M.G., A.H.Y. and A.F.; Data curation, M.G. and J.G.; Writing—original draft preparation, M.G. and J.G.; Writing—review and editing, E.D., J.G. and A.F.; Visualization, M.G. and A.H.Y.; Supervision, E.D. and A.F.; Project administration, M.G., V.P.N. and A.F.; Funding acquisition, A.F., J.G. and M.G. contributed equally to this paper. All authors have read and agreed to the published version of the manuscript.

Funding: This research was funded by the Ministry of Science and Technology of the State of Israel, grant no. 3-16652 and no. 3-16461. The APC was funded by the Schlesinger Family Center for Compact Accelerators, Radiation Sources, and Applications.

Data Availability Statement: The data presented in this study are available on request from the corresponding author. The data are not publicly available because they belong to the research and development part of a compact particle accelerator at the Schlesinger Family Center for Compact Accelerators, Radiation Sources and Applications (FEL).

Acknowledgments: We are thankful to the Ministry of Science and Technology of the State of Israel for the support of the project “Development of an Artificial Intelligence System for the Design of a Terahertz Optical Mode Converter”, grant no. 3-16652. In the field: applied science and engineering for students in the direct/combined third-degree program named after Ze’ev Jabotinsky. In addition, the authors would like to thank Yehiel Vashdi, the director of the Schlesinger Family Center for Compact Accelerators, Radiation Sources, and Applications, for their valuable help in the research.

Conflicts of Interest: The authors declare no conflict of interest.

References

1. Chamberlain, M.; Jones, B.; Wilke, I.; Williams, G.; Parks, B.; Heinz, T.; Siegel, P. Opportunities in THz Science. *Science* **2004**, *80*, 123.
2. Tripathi, S.R.; Miyata, E.; Ishai, P.B.; Kawase, K. Morphology of human sweat ducts observed by optical coherence tomography and their frequency of resonance in the terahertz frequency region. *Sci. Rep.* **2015**, *5*, 9071. [[CrossRef](#)]
3. Dalzell, D.R.; Mcquade, J.; Vincelette, R.; Ibey, B.; Payne, J.; Roach, W.P.; Roth, C.L.; Wilmink, G.J. Damage thresholds for terahertz radiation. In *Optical Interactions with Tissues and Cells XXI*; SPIE: St. Bellingham, WA, USA, 2010. [[CrossRef](#)]
4. Rauta, P.R.; Mohanta, Y.K.; Nayak, D. Nanotechnology in Biology and Medicine. *Nanotechnol. Biol. Med.* **2019**, *52*, 2438–2447. [[CrossRef](#)]
5. Li, J.; Zheng, C.; Wang, G.; Li, J.; Zhao, H.; Yang, Y.; Zhang, Z.; Yang, M.; Wu, L.; Li, J.; et al. Circular dichroism-like response of terahertz wave caused by phase manipulation via all-silicon metasurface. *Photonics Res.* **2021**, *9*, 567. [[CrossRef](#)]
6. Wang, P.; He, F.; Liu, J.; Shu, F.; Fang, B.; Lang, T.; Jing, X.; Hong, Z. Ultra-high-Q resonances in terahertz all-silicon metasurfaces based on bound states in the continuum. *Photonics Res.* **2022**, *10*, 2743. [[CrossRef](#)]
7. Chiang, W.-F.; Silalahi, H.M.; Chiang, Y.-C.; Hsu, M.-C.; Zhang, Y.-S.; Liu, J.-H.; Yu, Y.; Lee, C.-R.; Huang, C.-Y. Continuously tunable intensity modulators with large switching contrasts using liquid crystal elastomer films that are deposited with terahertz metamaterials. *Opt. Express* **2020**, *28*, 27676. [[CrossRef](#)]
8. Silalahi, H.M.; Chiang, W.-F.; Shih, Y.-H.; Wei, W.-Y.; Su, J.-Y.; Huang, C.-Y. Folding metamaterials with extremely strong electromagnetic resonance. *Photonics Res.* **2022**, *10*, 2215. [[CrossRef](#)]
9. Gershun, A. The Light Field. *J. Math. Phys.* **1939**, *18*, 51–151. [[CrossRef](#)]
10. Levoy, M. Light fields and computational imaging. *Computer* **2006**, *39*, 46–55. [[CrossRef](#)]
11. Friedman, A.; Balal, N.; Bratman, V.; Dyunin, E.; Lurie, Y.; Magory, E.; Gover, A. Configuration and status of the israeli THz free electron laser. In *Proceedings of the 36th International Free Electron Laser Conference, Basel, Switzerland, 25–29 August 2014*; pp. 553–555.

12. Dyunin, E.; Lurie, Y.; Pinhasi, Y.; Gover, A.; Marks, H. A new THz FEL development project. In Proceedings of the 2008 IEEE 25th Convention of Electrical and Electronics Engineers in Israel, Eilat, Israel, 3–5 December 2008; pp. 825–829. [CrossRef]
13. Haj Yahya, A.; Gerasimov, M.; Ciplis, J.; Balal, N.; Friedman, A. Determination of a High-Power THz Detector for EA-FEL Radiation Using Optical Sampling of GaAs and ZnTe Crystals. *Designs* **2022**, *6*, 109. [CrossRef]
14. Gerasimov, M.; Perutski, B.; Dyunin, E.; Gerasimov, J.; Friedman, A. Visualization of an Ultra-Short THz Beams with a Radiation Propagation Analysis of the Novel Israeli Free Electron Laser. *Computation* **2022**, *10*, 193. [CrossRef]
15. Gerasimov, M.; Dyunin, E.; Gerasimov, J.; Ciplis, J.; Friedman, A. Application of wigner distribution function for THz propagation analysis. *Sensors* **2022**, *22*, 240. [CrossRef]
16. Lavelle, J.; O’Sullivan, C. Beam shaping using Gaussian beam modes. *J. Opt. Soc. Am. A Opt. Image Sci. Vis.* **2010**, *27*, 350–357. [CrossRef] [PubMed]
17. Horowitz, O.; Gerasimov, M.; Lurie, Y.; Friedman, A. Study of the transmission line for Israeli THz free-electron radiation source. *Phys. Plasmas* **2022**, *29*, 113301. [CrossRef]
18. O’Sullivan, C.; Murphy, J.; Gradziel, M.; Lavelle, J.; Peacocke, T.; Trappe, N.; Curran, G.; White, D.; Withington, S. Optical Modelling using Gaussian Beam Modes for the Terahertz Band. In Proceedings of the Terahertz Technology and Applications II, San Jose, CA, USA, 24–29 January 2009; Volume 7215. [CrossRef]
19. Niles, S.; Blau, J.; Colson, W. Hermite-Gaussian decomposition of free electron laser optical fields. *Phys. Rev. Spec. Top.-Accel. Beams* **2010**, *13*, 030702. [CrossRef]
20. Gerasimov, J.; Balal, N.; Liokumovitch, E.; Richter, Y.; Gerasimov, M.; Bamani, E.; Pinhasi, G.A.; Pinhasi, Y. Scaled modeling and measurement for studying radio wave propagation in tunnels. *Electronics* **2021**, *10*, 53. [CrossRef]
21. Samad, M.A.; Choi, S.W.; Kim, C.S.; Choi, K. Wave Propagation Modeling Techniques in Tunnel Environments: A Survey. *IEEE Access* **2023**, *11*, 2199–2225. [CrossRef]
22. Lurie, Y.; Friedman, A.; Pinhasi, Y. Single pass, THz spectral range free-electron laser driven by a photocathode hybrid rf linear accelerator. *Phys. Rev. Spec. Top.-Accel. Beams* **2015**, *18*, 070701. [CrossRef]
23. Pinhasi, Y.; Lurie, Y.; Yahalom, A. Space-frequency model of ultrawide-band interactions in free-electron lasers. *Phys. Rev. E* **2005**, *71*, 036503. [CrossRef]
24. Wang, Y.; Wang, L.; Wu, G.; Yang, J.; An, W.; Yu, J.; Guo, Y. Disentangling Light Fields for Super-Resolution and Disparity Estimation. *IEEE Trans. Pattern Anal. Mach. Intell.* **2022**, *8828*, 1. [CrossRef]
25. Bastiaans, M.J. Wigner Distribution in Optics. 2009, pp. 1–42. Available online: <https://citeseerx.ist.psu.edu/document?repid=rep1&type=pdf&doi=f1041d8a956a08bfcaed136339d8986591ccb491> (accessed on 28 May 2023).
26. Wigner, E. On the quantum correction for thermodynamic equilibrium. *Phys. Rev.* **1932**, *40*, 749–759. [CrossRef]
27. Gao, H.; Tian, L.; Zhang, B.; Barbastathis, G. Iterative nonlinear beam propagation using Hamiltonian ray tracing and Wigner distribution function. *Opt. Lett.* **2010**, *35*, 4148–4150. [CrossRef]
28. Sheppard, C.J.R.; Larkin, K.G. Wigner function for nonparaxial wave fields. *JOSA A* **2006**, *18*, 2486–2490. [CrossRef]
29. Bastiaans, M.J. Wigner distribution function and its application to first-order optics. *J. Opt. Soc. Am.* **1979**, *69*, 1710. [CrossRef]
30. Bastiaans, M.J. Applications of the Wigner distribution to partially coherent light beams. *Adv. Inf. Opt. Photonics* **2008**, *6*, 27–56.
31. Tanner, G.; Ramapriya, D.M.; Gradoni, G.; Creagh, S.C.; Moers, E.; Arteaga, I.L. A Wigner function approach to near-field acoustic holography—Theory and experiments. In Proceedings of the INTER-NOISE 2019 MADRID—48th International Congress and Exhibition on Noise Control Engineering, Madrid, Spain, 16–19 June 2019.
32. Dragoman, D. Applications of the Wigner Distribution Function. *EURASIP J. Adv. Signal Process.* **2005**, *2005*, 264967. [CrossRef]
33. Feature, T.D. Robust Radar Emitter Recognition Based on the Three-Dimensional Distribution Feature and Transfer Learning. *Sensors* **2016**, *16*, 289. [CrossRef]
34. Guner, K.K.; Gulum, T.O.; Erkmn, B. FPGA-Based Wigner-Hough Transform System for Detection and Parameter Extraction of LPI Radar LFM CW Signals. *IEEE Trans. Instrum. Meas.* **2021**, *70*, 1–15. [CrossRef]
35. Orović, I.; Stanković, S.; Draganić, A. Time-frequency based analysis of wireless signals. In Proceedings of the 2012 Mediterranean Conference on Embedded Computing (MECO), Bar, Montenegro, 16–19 June 2012; pp. 92–95.
36. Stern, A.; Javidi, B. Sampling in the light of Wigner distribution: Errata. *J. Opt. Soc. Am. A* **2004**, *21*, 2038. [CrossRef]
37. Alonso, M. Exact description of free electromagnetic wave fields in terms of rays. *Opt. Express* **2003**, *11*, 3128. [CrossRef]
38. Jepsen, P.U.; Cooke, D.G.; Koch, M. Terahertz spectroscopy and imaging—Modern techniques and applications. *Laser Photonics Rev.* **2011**, *5*, 124–166. [CrossRef]
39. Lakshminarayan, V.; Calvo, M.L.; Alieva, T. *Mathematical Optics: Classical, Quantum, and Computational Methods*; CRC Press: Boca Raton, FL, USA, 2018; pp. 13–51.
40. Cámara, A.; Rodrigo, J.A.; Alieva, T. Optical coherenscopy based on phase-space tomography. *Opt. Express* **2013**, *21*, 13169. [CrossRef]
41. Nash, B.; Goldring, N.; Edelen, J.; Webb, S.; Llc, R.; Lane, M. Propagation of partially coherent radiation using Wigner functions. *Phys. Rev. Accel. Beams* **2021**, *24*, 10702. [CrossRef]
42. Zhang, Z.; Levoy, M. Wigner distributions and how they relate to the light field. In Proceedings of the 2009 IEEE International Conference on Computational Photography (ICCP), San Francisco, CA, USA, 16–17 April 2009.

43. Son, J.; Mandracchia, B.; Caponegro, M.D.; Tsirka, S.E.; Jia, S. BSSE: An open-source image processing tool for miniaturized microscopy. *Opt. Express* **2019**, *27*, 17620–17637. [[CrossRef](#)]
44. Kwon, K.; Park, C.; Erdenebat, M.; Jeong, J.; Kim, N.; Park, J.; Lim, Y.; Yoo, K. High speed image space parallel processing for computer-generated integral imaging system. *Opt. Express* **2012**, *20*, 732–740. [[CrossRef](#)]

Disclaimer/Publisher’s Note: The statements, opinions and data contained in all publications are solely those of the individual author(s) and contributor(s) and not of MDPI and/or the editor(s). MDPI and/or the editor(s) disclaim responsibility for any injury to people or property resulting from any ideas, methods, instructions or products referred to in the content.